

Received July 29, 2021, accepted August 5, 2021, date of publication August 11, 2021, date of current version August 19, 2021.

Digital Object Identifier 10.1109/ACCESS.2021.3103977

Analysis on Circulating Current Loss in the Formed Winding of Permanent Magnet Synchronous Motors

JIA LIU, YANPING LIANG[✉], PEIPEI YANG, WEIHAO WANG, FUCHAO ZHAO, AND KANGWEN XU

College of Electrical and Electronic Engineering, Harbin University of Science and Technology, Harbin 150080, China

Corresponding author: Yanping Liang (liangyanping2010@126.com)

This work was supported in part by the National Natural Science Foundation of China under Grant 51977053.

ABSTRACT Permanent magnet synchronous motors with the formed winding can not only improve the slot fill factor and heat dissipation capacity but also effectively reduce the additional loss in the winding. Formed winding permanent magnet synchronous motors will become the future development tendency. Due to inherent features of the formed winding, the circulating current loss is a non-negligible issue. This paper proposes using the formed winding in permanent magnet synchronous motors and analyzes the circulating current loss in the formed winding. First, the finite element models of integer slot and fractional slot motors are established, and the magnetic field analysis are carried out. Then two commonly used methods of calculating circulating current loss are introduced in detail, and their calculation results are compared. Moreover, the high-precision field-circuit coupled finite element method is used to calculate the circulating current loss of integer and fractional motors. And circulating currents of the hairpin winding and the formed winding are compared. The analysis indicates that the circulating current in the formed winding cannot be ignored. Finally, comprehensive and in-depth research on the influencing factors of circulating current loss in the formed winding has been conducted. The results clarify that the number of parallel strands, the width of the slot opening, and the stator current have a considerable influence on the circulating current loss.

INDEX TERMS Circulating current loss, field-circuit coupling, permanent magnet synchronous motors, slot-pole combination, the formed winding.

I. INTRODUCTION

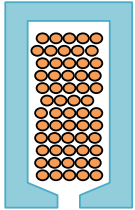
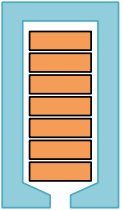
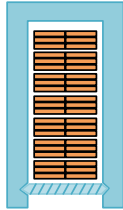
In recent years, the rapid development of electric vehicles (EVs) and aerospace has put forward higher requirements of different types of electrical machines, including permanent magnet synchronous motors (PMSM), switched reluctance motors (SRM), induction motors (IM) and so on [1]–[3]. Compared with PMSM, the torque ripple of SRM is larger, the efficiency of IM is smaller, and the power density of SRM and IM is relatively low [3], [4]. An ever-increasing use of PMSM in high-performance sectors such as electric vehicles has been observed due to their advantages of high power density and high efficiency. More and more scholars pay attention to PMSM, which causes PMSM to become a research hotspot. PMSM mostly use the round copper wire winding or the hairpin winding type. The round copper wire winding has low slot fill factor and poor heat dissipation

capacity. The hairpin winding can effectively improve the slot fill factor [5], [6]. But the hairpin winding has a large eddy current loss due to its large cross-sectional area [7]–[10]. The eddy current loss in the hairpin winding needs to be solved urgently. Therefore, this paper proposes using the formed winding in PMSM. The formed winding composed of double rows of multiple parallel flat wires is a new type of winding technology in PMSM. Winding types of PMSM are shown in Table 1, and physical images are shown in Fig. 1. Using the formed winding in PMSM can increase the slot fill factor and reduce eddy current loss. So, the formed winding PMSM is likely to become the future development tendency.

While the formed winding in PMSM has numerous merits, it also presents drawbacks such as circulating current. The uneven distribution of the leakage magnetic field will cause the potential difference between parallel strands in the formed winding [11], [12]. This phenomenon directly leads to the circulating current loss [13]. Previous literatures

The associate editor coordinating the review of this manuscript and approving it for publication was Jinquan Xu[✉].

TABLE 1. Winding types of PMSM.

	Round copper wire winding	Hairpin winding	Formed winding
Geometry			
Slot opening type of stator	Semi-closed slot	Semi-closed slot	Open slot
Assembly of coils	Mounting in radial direction	Mounting by axial inserting	Mounting in radial direction
Type of end connection	Coil of wire	Forming and welding	Parallel joint
Embedding difficulty	Most difficult	More difficult	Simple

on the circulating current loss mainly focused on the stator bar of large AC motors or the parallel branches in PMSM. Reference [14], [15] illustrated that circulating current exists in motors with multiple parallel branches. Circulating current loss affects the efficiency and the temperature rise of the stator [16], [17]. Reference [18] proposed end transposition to reduce the circulating current of tooth-wound coils. References [19] proposed a global transposition to reduce the circulating current in the stator bar of a large AC motor. The formed winding is a newly proposed winding technology in PMSM, the loss mechanism caused by the formed winding of PMSM is different from that of existing windings. It is rare in existing literatures to study the circulating current loss between the parallel strands in the formed winding of PMSM.

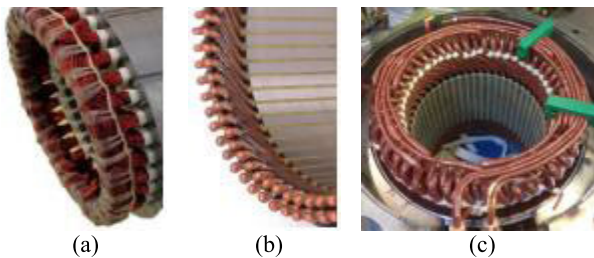


FIGURE 1. The physical images of winding types [3]. (a) Round copper wire winding (b) Hairpin winding (c) Formed winding.

At the initial moment of motor design, considering the circulating current loss is necessary. Analyzing influencing factors of the circulating current loss is helpful to PMSM designers at the beginning of design. References [20]–[22] showed that the position and number of strands, the voltage, and the speed all impact the circulating current loss of the round wire winding PMSM. The accurate calculation of circulating current loss is essential to design the motor and select the transposition type. References [23] calculated the circulating current loss of large AC motors by analytical method. Large AC motors are large in size and difficult to analyze by finite element, so most of them calculate

circulating current by analysis method. The calculation speed of the analytical method is 18 times faster than the finite element method [24]. But analytical method made a lot of simplifications and set inaccurate boundary conditions, so it is not suitable for general application compared with the finite element method [20]. Reference [11], [16], [18], [20]–[22] used the 2D finite element method to analyze the circulating current loss of the round wire PMSM, and reference [16], [18] verified the effectiveness of the finite element method by experiments.

The first task of motor design is to select a suitable slot-pole combination. Slot-pole combinations play an essential role in the manufacture and performance of PMSM [25]. Integer slot motors have low rotor loss but large cogging torque. In contrast, fractional slot motors have small cogging torque but high magnetomotive force harmonic [26]–[28]. The magnetic flux generated by the stator current in the air gap is about half of the magnetic flux generated by the permanent magnet [29]. Different winding arrangements impact the electromagnetic performance. The difference in the electromagnetic performance will affect the circulating current loss.

In this paper, the circulating current loss in the formed winding of PMSM is studied. Two finite element models of PMSM with different slot-pole combinations are established, and their magnetic fields are analyzed. Then two generally used calculation methods for circulating current loss, the leakage inductance potential method and the field-circuit coupling method, are introduced in detail, and their calculation results are compared. The field-circuit coupling method is used to calculate the circulating current loss of integer slot and fractional slot PMSM. And the circulating current loss of the hairpin winding and the formed winding are compared. The results show that the circulating current loss distribution of PMSM with different slot-pole combinations is not the same, and the circulating current in the formed winding cannot be ignored. In view of this phenomenon, influencing factors of circulating current loss in the formed winding are studied at great length.

II. THE FORMED WINDING OF PMSM

A. THE FORMED WINDING

The formed winding in PMSM draws lessons from the stator bar technology in large AC motors. The formed winding is made up of multiple flat copper wires, including a straight section and two ends. And PMSM with the formed winding adopts rectangular open slot stator structure. The formed winding is embedded through the slot opening and connected at the end through the parallel joint to form a complete coil. The schematic diagram of the formed winding is shown in Fig. 2. The formed winding is different from the existing winding types of PMSM. Although it has a non-negligible circulating current loss, it can reduce circulating current loss by transposing strands and changing the end connection mode. The manufacture of the formed winding is more complicated, but its application in PMSM is convenient to embed. Most

importantly, the formed winding in PMSM can improve the slot fill factor and heat dissipation capacity and can reduce additional losses.

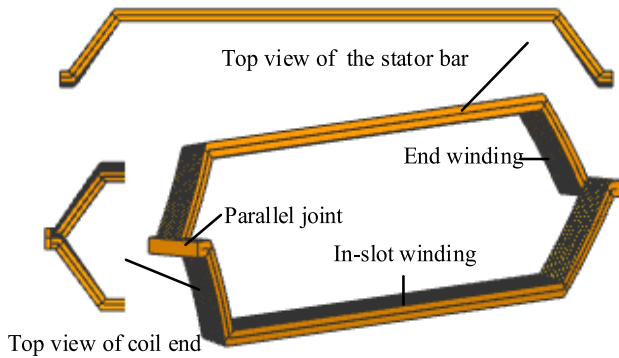


FIGURE 2. The schematic diagram of the formed winding.

The formed winding PMSM can be classified by different classification principles. According to the number of slots per pole per phase, the formed winding PMSM can be divided into integer slot PMSM and fractional slot PMSM. The number of slots per pole per phase can be expressed as

$$q = \frac{Q}{2pm} \quad (1)$$

where Q is the number of stator slots, p is the number of pole pairs, m is the number of phases. When q is an integer, it is an integer slot PMSM, otherwise it is a fractional slot PMSM.

B. INTEGER SLOT AND FRACTIONAL SLOT PMSM

This paper takes a 12-pole integer slot formed winding PMSM as an example. According to the principle of the same rotor and the same power density, a fractional slot formed winding PMSM is designed. The one-sixth model of two PMSM is shown in Fig. 3. The main parameters of two PMSM are shown in Table 2. Compared with the integer slot PMSM, the structural parameters of the fractional slot motor are basically unchanged, only the winding parameters change.

TABLE 2. Main parameters of formed winding PMSM.

Parameters	Integer slot	Fractional slot
Rated power (kW)	105	105
Rated current (A)	188.3	157.5
Stator inner diameter (mm)	260	260
Core length (mm)	200	200
Number of stator slots	72	54
pitch	5	4
Conductors per slot	4	6
Parallel number	10	8

To save calculation time, the influence of the end leakage magnetic field is ignored. 2D finite element models of two motors are set up and analyzed. The no-load magnetic density distributions are shown in Fig. 4. Due to the thinner

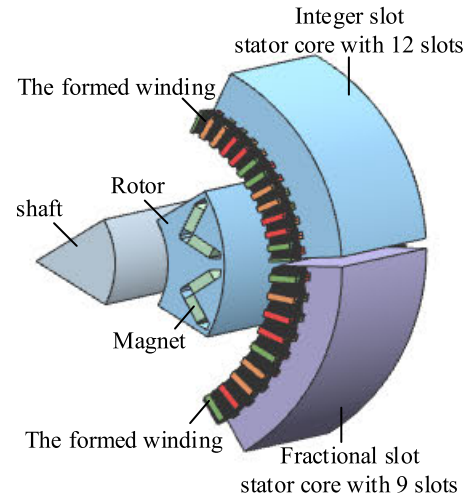


FIGURE 3. One-sixth model of formed winding PMSM.

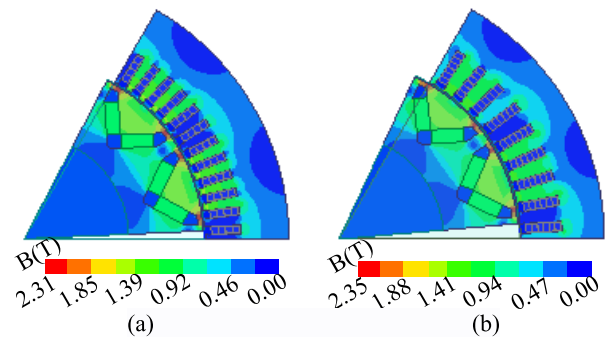


FIGURE 4. No-load magnetic density cloud map of the formed winding PMSM. (a) Integer slot. (b) Fractional slot.

rotor tip and stator teeth, the maximum magnetic density of both appear at the top of the rotor and the stator teeth. The maximum flux density of the fractional slot motor is 2.35T, greater than that of the integer slot motor. But the stator teeth magnetic density of the fractional slot motor is slightly smaller. The no-load magnetic leakage coefficient of the motor is

$$\sigma_0 = \frac{\Phi_m}{\Phi_\delta} \quad (2)$$

where Φ_m is total flux per pole, the rotor magnetic circuit structure remains unchanged, Φ_m is unchanged. Φ_δ is the air gap flux per pole, and the expression is

$$\Phi_\delta = \int_0^\tau B_{\delta 1} \sin \frac{\pi x}{\tau} dx \cdot L_1 \quad (3)$$

where τ is the pole pitch, $B_{\delta 1}$ is the fundamental wave amplitude of air gap magnetic density, L_1 is the core length. Stator inner diameter is constant, pole pitch has not changed.

The air gap magnetic density and Fourier decompositions under no-load condition are shown in Fig. 5. It can be seen from Fig. 5 (a) that the degree of the sine of the waveform is not perfect. The waveform of the integer slot PMSM is symmetrical along the magnetic pole centerline. But the

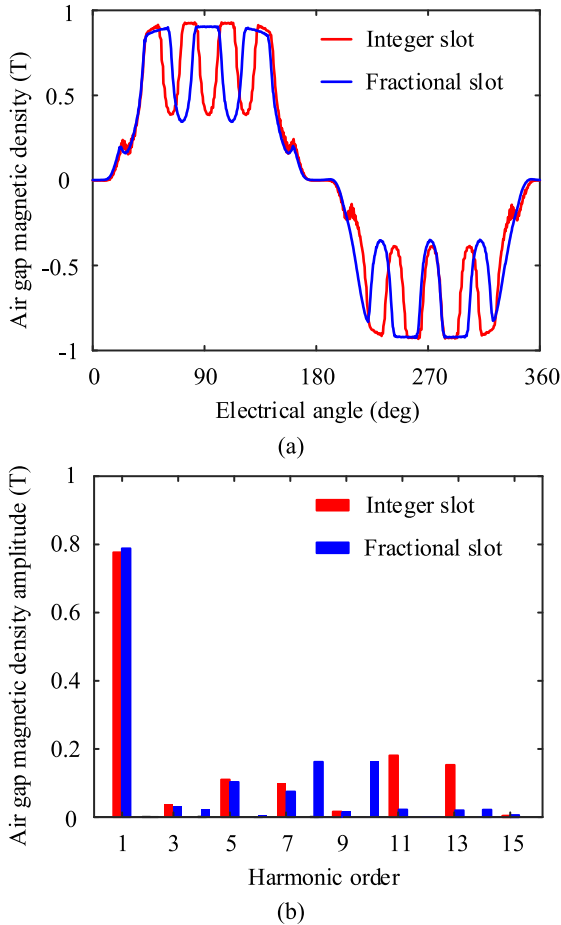


FIGURE 5. No-load air gap magnetic density waveforms and Fourier decompositions. (a) Waveforms. (b) Fourier decompositions.

waveform symmetry of the fractional slot PMSM is not good. Fig. 5 (b) is the frequency domain waveform obtained by Fourier decomposition. The fundamental wave amplitude of the integer slot PMSM is 0.78T, and the harmonic distortion rate is 19.75%. The fundamental wave amplitude of the fractional slot PMSM is 0.79T, and the harmonic distortion rate is 26.60%, which is all greater than that of the integer slot PMSM. On the basis of formulas (2) and (3), when the fundamental wave amplitude of the air gap magnetic density changes, the no-load magnetic leakage coefficient changes accordingly. So, the slot leakage magnetic field distribution of PMSM with different winding arrangements is different.

When PMSM adopts the formed winding, the uneven distribution of leakage magnetic field and the relative position difference between strands will lead to differences in the size of the magnetic chain of different branches. It causes that the leakage electromotive force induced by each strand is different. There is a potential difference between the strands, which generates circulating current. The winding arrangement affects the leakage magnetic field in the slot of PMSM, resulting in the different circulating current distribution.

III. CALCULATION METHOD OF CIRCULATING CURRENT LOSS AND RESULT ANALYSIS

Due to the uneven distribution of the leakage magnetic field and the inherent structural features of the formed winding, the circulating current flow path generates between parallel strands. Calculating circulating current loss is vital for designing the motor and choosing the transposition type. Calculation methods of circulating current loss include the analytical method and field-circuit coupling method. The analytical method calculates fast but uses many empirical coefficients and assumptions, and the calculation process is cumbersome. In contrast, the field-circuit coupling finite element method has high accuracy but requires accurate modeling and a long calculation time.

A. LEAKAGE INDUCTANCE ELECTROMOTIVE FORCE METHOD

The leakage inductance electromotive force method is a commonly used analytical method to calculate the circulating current loss. Due to the uneven distribution of the slot and the end leakage magnetic field, there is a potential difference between the strands cause the circulating current. So, leakage inductance electromotive force is divided into the slot and end leakage inductance electromotive force. The winding in the slot interlinks with the leakage flux to generate the slot leakage electromotive force. The end winding and the leakage flux are linked to produce the end leakage electromotive force. Precisely calculating the leakage inductance electromotive force is the key to calculate the circulating current.

Make the following assumptions:

- 1) The resistance of each strand is the same.
- 2) Ignore the saturation of the stator core.
- 3) The strand current changes with time and the strand current at the initial moment is the average value of the stator current, that is, $I_i^{(0)}$.

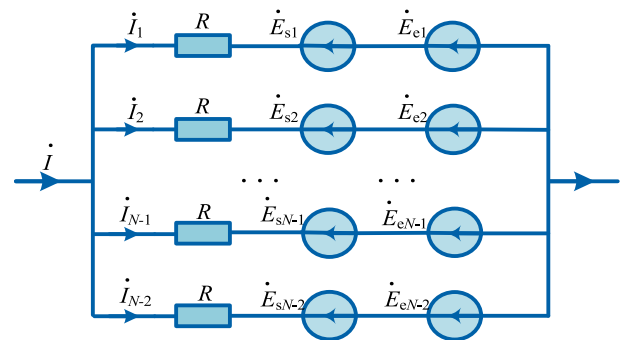


FIGURE 6. Equivalent circuit of leakage inductance potential method.

The equivalent circuit for calculating the circulating current loss is shown in Fig. 6. Each strand is equivalent to a strand resistance (R), a slot leakage inductance electromotive force (\dot{E}_{si}) and an end leakage inductance electromotive force (\dot{E}_{ei}). Each turn of the stator bar is formed by N strands. I_i is the total current flowing through each turn of the stator bar. \dot{I}_i

is the current effective value vector of the i -th strand in each turn of the stator bar, expressed as $\dot{I}_i = I_i \angle \varphi_i$. I_i is the effective value of the i -th strand current, φ_i is the current phase angle. The formulas used in this part referred to [22].

The Ampere's loop law is expressed as

$$\oint_l \dot{H}_i dl = \int_{b_s} \frac{\dot{B}_i}{\mu_0} dl = \dot{I}_i \quad (4)$$

where \dot{H}_i is the magnetic field intensity, \dot{B}_i is the magnetic induction intensity, b_s is the slot width.

The magnetic induction intensity can be expressed as

$$\dot{B}_i = \frac{\mu_0 \dot{I}_i}{b_s} \quad (5)$$

where μ_0 is vacuum permeability, $\mu_0 = 4\pi \times 10^{-7} \text{N} \cdot \text{A}^{-2}$.

Then the self-inductance leakage flux of the i -th strand is

$$\dot{\Phi}_{ii} = \int \dot{B}_i dS = \dot{B}_i S_{ii} \quad (6)$$

where S_{ii} is the area of self-inductance leakage flux linkage.

The effective value vector of the self-induced electromotive force of the i -th strand is

$$\dot{E}_{ii} = -j\sqrt{2}\pi f \dot{\Phi}_{iim} = -j\frac{2\pi f \mu_0}{b_s} S_{ii} \dot{I}_i \quad (7)$$

where $\dot{\Phi}_{iim}$ is the amplitude vector of the self-inductance leakage flux, f is the frequency.

The angle of the self-induced electromotive force is 90° behind that of the current. The effective value vector of the mutual inductance electromotive force of the i -th strand is

$$\dot{E}_{ij} = -j\frac{2\pi f \mu_0}{b_s} S_{ij} \dot{I}_j \quad (8)$$

where S_{ij} is the slot leakage flux area, \dot{I}_j is the j -th strand current, $\dot{I}_j = I_j \angle \varphi_j$.

The expression of the stator slot leakage electromotive force of the i -th strand is

$$\dot{E}_{si} = \sum_{j=1}^{2N} \dot{E}_{ij} = -j\frac{2\pi f \mu_0}{b_s} \sum_{j=1}^{2N} (-jS_{ij} \dot{I}_j) \quad (9)$$

End strands are affected by the ferromagnetic boundary. The mirror image method is used to analyze the magnetic misalignment at the end strand. The schematic diagram of the end strand mirror method is shown in Fig. 7. In Fig. 7, ab and fg are the end extensions of the i -th strand in the upper layer and the j -th strand in the lower layer, respectively. The mirror plane is at the axial coordinate equal to 0. The mirror current of the j -th strand is

$$\dot{I}_1 = \frac{\mu_{Fe} - 1}{\mu_{Fe} + 1} \dot{I}_j \quad (10)$$

where μ_{Fe} is the core permeability. Ignoring the core saturation, the core permeability is infinite, so the mirror current is $\dot{I}_1 = \dot{I}_j$.

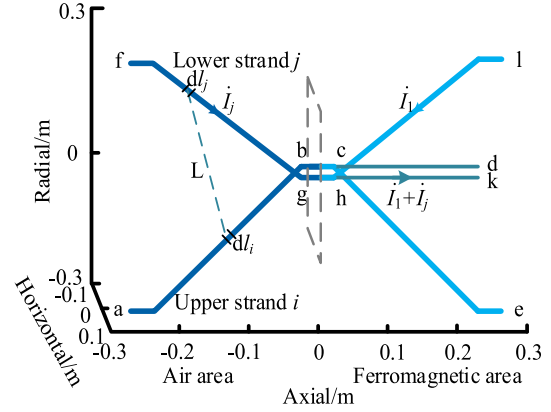


FIGURE 7. Schematic diagram of the mirror method at the end strand.

The magnetic flux of the alternating magnetic field that is generated by the j -th strand and its mirror current and the i -th strand expressed as

$$\dot{\Phi}_{ij} = \oint_l \dot{A}_{ij} \cdot dl_i \quad (11)$$

where \dot{A}_{ij} is the magnetic misalignment generated by the current at the micro-element dl_i of the i -th strand, and the expression is

$$\dot{A}_{ij} = \frac{\mu_0}{4\pi} \left(\int_{fgh} \frac{\dot{I}_j}{L} dl_j + \int_{lgh} \frac{\dot{I}_1}{L} dl_j + \int_{hkl} \frac{\dot{I}_1 + \dot{I}_j}{L} dl_j \right) \quad (12)$$

where L is the distance between dl_i and dl_j . The induced potential generated by the alternating magnetic field generated by the current \dot{I}_j at the end of the i -th strand is

$$\dot{E}_{ij} = -j\sqrt{2}\pi f \dot{\Phi}_{ijm} = -j\mu_0 f \dot{I}_j C_{ij} \quad (13)$$

where $C_{ij} = \int_{ab} \left(\int_{fgh} \frac{1}{2L} dl_j + \int_{lgh} \frac{1}{2L} dl_j + \int_{hkl} \frac{1}{L} dl_j \right) \cdot dl_i$, \dot{E}_{ij} lag the argument of $\dot{\Phi}_{ijm}$ by 90° . The end leakage inductance potential of the i -th strand is expressed as

$$\dot{E}_{ei} = \sum_{j=1}^{2N} \dot{E}_{ij} = \mu_0 f \sum_{j=1}^{2N} (-j\dot{I}_j C_{ij}) \quad (14)$$

Each turn of the stator bar is paralleled by N strands, and the total current passing through each turn of the bar is \dot{I} . The equivalent circuit diagram of the stator bar in Fig. 6. Iterative method can be used to solve the current in the i -th strand. The initial voltage of the i -th strand is expressed as

$$\dot{U}_i^{(0)} = R\dot{I}_i^{(0)} - \dot{E}_{si}^{(0)} - \dot{E}_{ei}^{(0)} \quad (15)$$

where R is the resistance of the strand, $\dot{I}_i^{(0)}$ is the initial strand current, that is, the average value of the stator current, $\dot{E}_{si}^{(0)}$ is the slot leakage inductance electromotive force at the initial moment, $\dot{E}_{ei}^{(0)}$ is the end leakage inductance electromotive force at the initial moment.

The average voltage of each strand is expressed as

$$\dot{U}_{av}^{(0)} = \frac{1}{N} \sum_{i=1}^N \dot{U}_i^{(0)} \quad (16)$$

where $\dot{U}_i^{(0)}$ is the strand voltage at the initial moment.

The voltage difference $\dot{U}_i^{(k)}$ of each strand and its average $\dot{U}_{av}^{(k)}$ can be obtained by iteratively calculating. According to formula (9), formula (13) and formula (14), the current of each strand can be calculated.

The circulating current in each strand is expressed as

$$\dot{i} = \dot{I}_j - \dot{I}_{av} \tag{17}$$

where \dot{I}_j is the effective value of the j -th strand current, \dot{I}_{av} is the average value of the strand current.

The circulating current loss of each parallel strand is

$$p_{cc} = |\dot{I}_{ki}|^2 R_{ki} \tag{18}$$

where \dot{I}_{ki} is the circulating current in the i -th strand, R_{ki} is the resistance of the i -th strand.

B. FIELD-CIRCUIT COUPLING METHOD

The leakage inductance electromotive force method not only ignore the saturation of the stator core, but also need to solve a series of equations to calculate the strand current. The analytical method has poor accuracy, and the solution process is more complicated. The field-circuit coupling method can make up for the deficiencies of the analytical method. The field-circuit coupling method is simpler, and the calculation result is more accurate, but model accuracy and computing time are more demanding.

The field-circuit coupling method is based on finite element software, and parallel strands are equivalent to a parallel circuit network, and each strand constitutes a branch circuit. The ends of each branch are connected together in parallel, and then the ‘‘electromagnetic field-circuit’’ coupling solution for calculating the circulating current loss is realized. The field-circuit coupling method is used to get the current distribution of each parallel strand.

The calculation of 3D finite model requires much time. The application of 2D finite element analysis of the magnetic field in the slot has higher accuracy. This article ignores the end leakage magnetic field, establishes 2D finite element models, and uses external circuit to be equivalent to the end connection. The pitch of the integer slot PMSM is 5, take No. 1 slot winding as an example, the No. 1 upper winding is connected to the No. 6 lower winding. The calculation model and equivalent external circuit are shown in Fig. 8 and Fig. 9. In Fig. 8, PQ satisfies the Vector Potential boundary condition, ON satisfies the Neumann boundary condition, OP and OQ satisfy the periodic boundary condition. And boundary conditions satisfied by the calculation model can be expressed as

$$A|_{PQ} = 0 \tag{19}$$

$$\frac{\partial A}{\partial n} \Big|_{ON} = 0 \tag{20}$$

$$A|_{OP} = A|_{OQ} \tag{21}$$

where n is the normal direction of the geometric neutral between the magnetic poles.

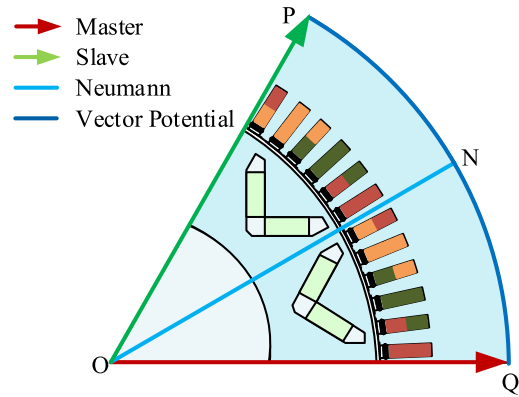


FIGURE 8. The calculation model of the formed winding PMSM.

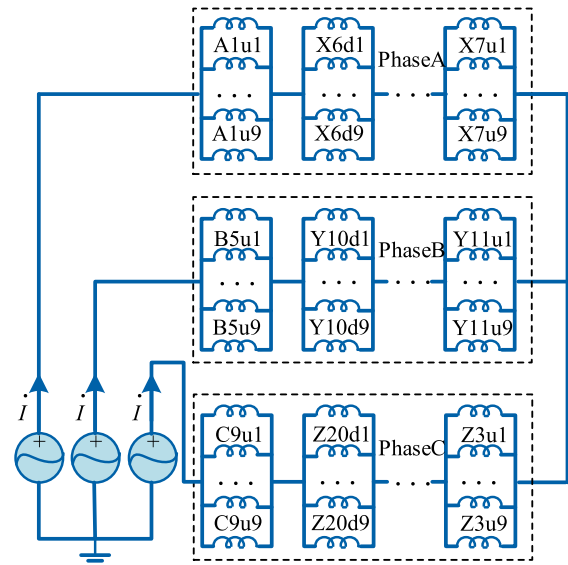


FIGURE 9. Equivalent external circuit of field-circuit coupling method.

In order to facilitate subsequent analysis, the strands of the formed winding are numbered. The lower winding is numbered in the same way as the upper winding. The strand number are shown in Fig. 10. The integer slot PMSM and the fractional slot PMSM under rated operating conditions are simulated separately. Using finite element software to analyze can get the current of each parallel strands. And then equations (17) and (18) are applied to obtain the circulating current loss distribution.

C. COMPARISON OF THE RESULTS CALCULATED BY THE TWO CALCULATION METHODS

The leakage inductance potential method and the field-circuit coupled finite element method are commonly used to calculate the circulating current loss. In order to verify the accuracy of the calculation results, the current of each strand in the integer slot and the fractional slot PMSM calculated by the two methods are compared.

This paper aims to analyze the influence of the slot leakage magnetic on circulating current in PMSM. The 2D finite element method is accurate and fast to analyze the slot leakage

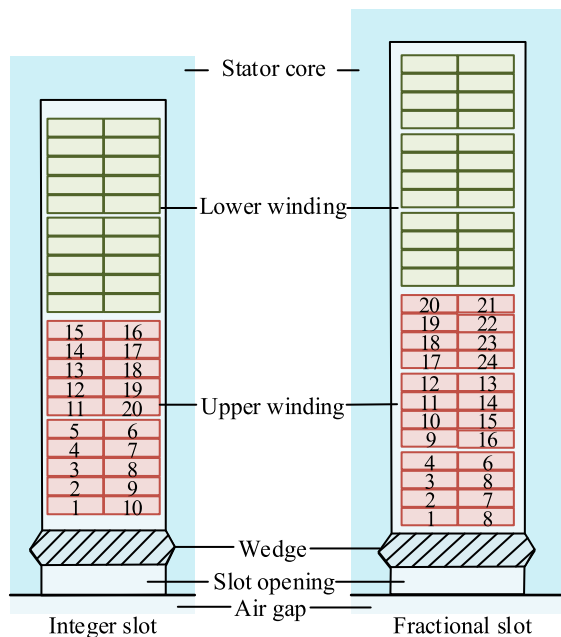


FIGURE 10. The strand number of the formed winding PMSM.

magnetic flux, so the 2D finite element method is applied to analyze the circulating current. And to accurately compare the finite element method and the analytical method to calculate the circulating current, only the slot leakage magnetic field is considered when applying the leakage inductance potential method.

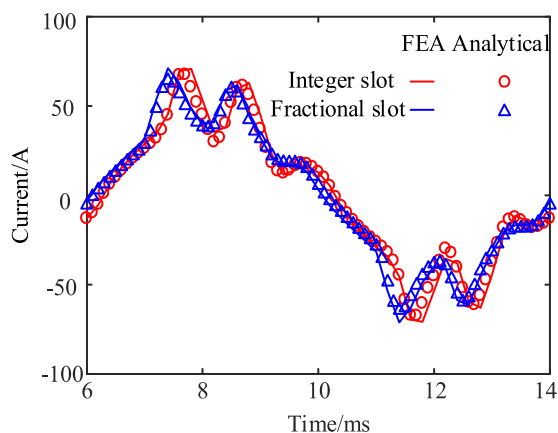


FIGURE 11. The current of the No. 1 strand in two PMSM.

The current distributions of the No. 1 strand near the slot notch in two PMSM in one period are shown in Fig. 11. It can be seen from Fig. 11 that the finite element method and the analytical method are in good agreement. However, due to the assumptions and different calculation steps used in the analytical method, there are still small differences between the two methods.

The prerequisite for the accurate calculation of the circulating current by the leakage inductance potential method is the precise calculation of the leakage magnetic field. But the process of applying the analytical method to calculate the

leakage magnetic field is cumbersome and has poor accuracy. The field-circuit coupling method needs exact modeling, accurate setting of boundary and excitation, and reasonable mesh. Besides, the better computer performance and longer computing time are required. But the field-circuit coupling method has high accuracy.

D. ANALYSIS OF THE RESULTS CALCULATED BY THE FIELD-CIRCUIT COUPLING FINITE ELEMENT METHOD

The field-circuit coupling method based on finite element software and the current of each strand can be directly obtained. Although the field-circuit coupling method needs accurate modeling, high computer hardware, and long calculation time. But the field-circuit coupling method has high accuracy, the 2D PMSM finite element model is small, and the computer is well developed, so the field-circuit coupling method is used in the following research.

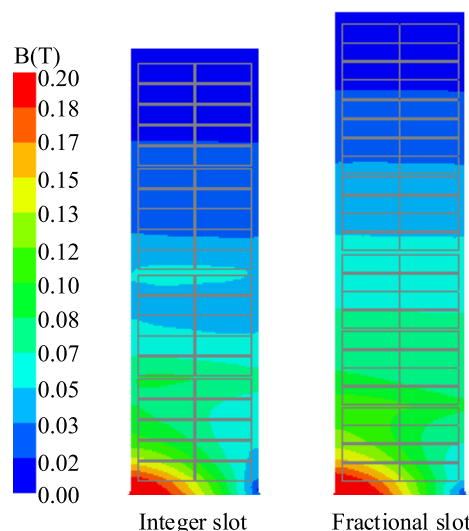


FIGURE 12. Magnetic density distribution in the slot.

Magnetic density distribution in the slot are shown in Fig. 12. It can be seen from Fig. 12 that the overall magnetic density distribution in the integer slot and the fractional slot motor is similar. The strands closer to the slot notch are more affected by the leakage magnetic field, and the strands farther away from the slot notch are less affected. In the same slot height direction, the parallel strands closest to the slot notch are affected by the leakage magnetic field differently. The closer to the slot bottom, the smaller the magnetic density and the more uniform the magnetic density distribution. The circulating current loss distribution of integer slot and fractional slot PMSM obtained by the field-circuit coupling method are shown in Fig. 13 and Fig. 14. The circulating current loss of the lower winding is much smaller than that of the upper winding. One turn stator bar near the slot notch in the upper winding is affected differently by the leakage magnetic field. Except for one turn stator bar near the slot notch, the circulating current loss of the strands shows a “W”-shaped distribution.

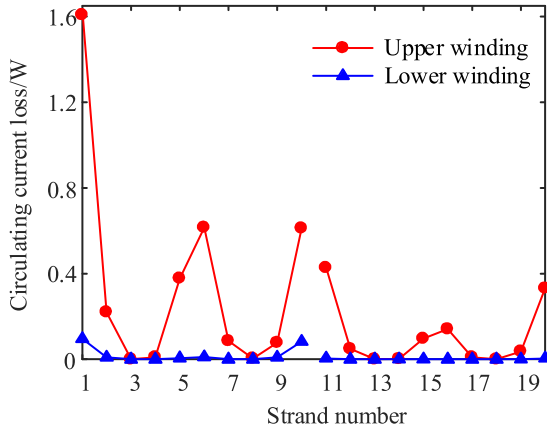


FIGURE 13. Circulating current loss distribution in strands of the integer slot formed winding PMSM.

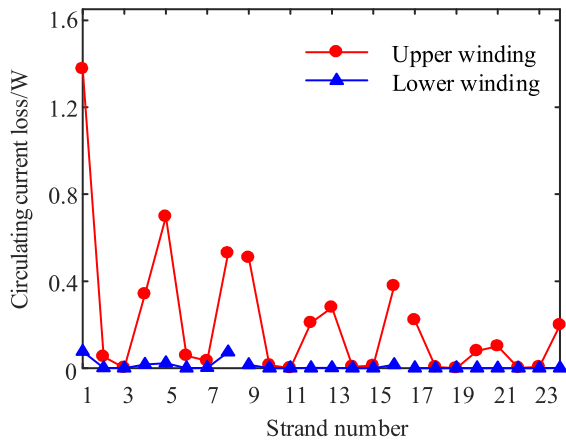


FIGURE 14. Circulating current loss distribution in strands of the fractional slot formed winding PMSM.

The maximum value of the circulating current loss of the strand in the integer slot PMSM is greater than that of the fractional slot PMSM. The circulating current loss in one slot of the integer slot PMSM is about 4.94W, which is less than the 5.33W of the fractional slot PMSM. However, the total circulating current loss of the integer slot PMSM is 355.68W, which is much larger than the total circulating current loss of the fractional slot PMSM of 287.82W. The winding arrangement type has a considerable influence on the circulating current loss of the formed winding PMSM.

Regardless of whether it is the integer slot PMSM or the fractional slot PMSM, the circulating current loss in the formed winding cannot be ignored. Compared with the round wire winding, the hairpin winding and the formed winding have obvious advantage of high slot fill factor. However, the parallel strands of the round wire winding are very thin and easily transposed during the wire winding, so the eddy current loss and circulating current loss in the round wire winding are very small and almost zero. Eddy current loss and circulating current loss are collectively referred to as AC copper loss. The AC copper loss in the hairpin winding and the formed winding is relatively large. Equivalent external circuit of the hairpin winding is shown in Fig. 15. The hairpin

winding passes through all positions in the slot, and the number of parallel branches is 1.

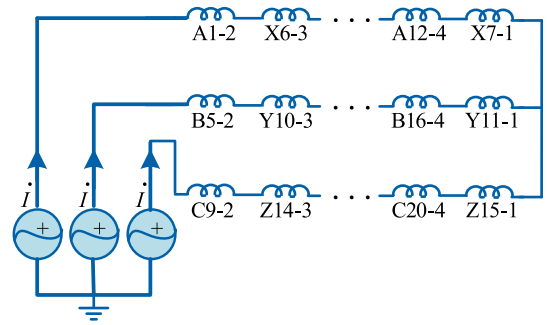


FIGURE 15. Equivalent external circuit of the hairpin winding.

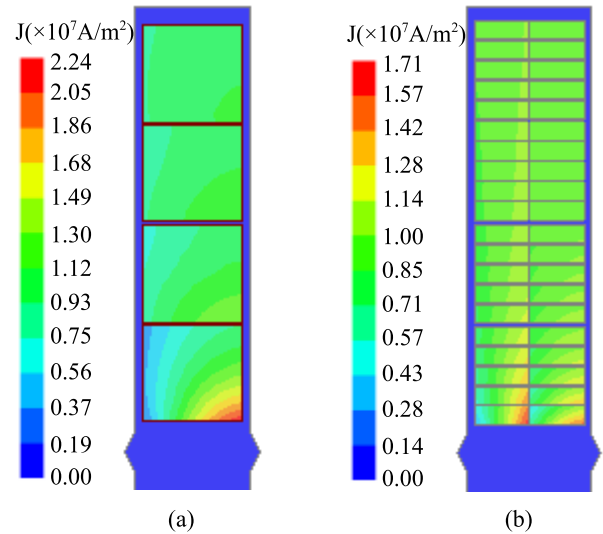


FIGURE 16. Electric density distribution of the hairpin winding and the formed winding. (a) The hairpin winding. (b) The formed winding.

Fig. 16 shows the electric density of the hairpin winding and the formed winding. The cross-sectional area of the formed winding is reduced, and its maximum electric density is smaller than that of the hairpin winding. The eddy current loss is proportional to the square of the electric density, so the eddy current loss in the formed winding is much smaller than the hairpin winding.

The circulating current distributions of the strand closest to the slot notch of the hairpin winding and the formed winding are shown in Fig. 17. The circulating current of the formed winding is larger, and that of the hairpin winding is almost zero. The number of parallel branches of the hairpin winding is 1, the hairpin winding with 1 parallel branch have no circulating current loss. There is a phase difference between the strand current with the circulating current and the strand current without the circulating current of the formed winding, so the waveform of the circulating current is different from the strand current.

AC copper losses of the hairpin winding and the formed winding are shown in TABLE 3. Both the hairpin winding

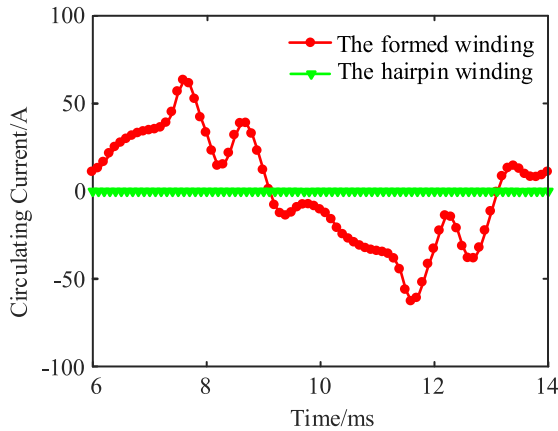


FIGURE 17. Circulating current of hairpin winding and formed winding.

and the formed winding can effectively increase the slot fill factor, but the AC copper loss is large. Compared with the hairpin winding, the formed winding can reduce eddy current loss. Even if there is circulating current loss in the formed winding, the total AC copper loss is still less than that of the hairpin winding.

TABLE 3. AC copper losses of the hairpin winding and the formed winding.

Winding type	Eddy current loss(W)	Circulating current loss(W)	Total AC copper loss (W)
The hairpin winding	2200.70	0	2200.70
The formed winding	1404.40	355.68	1767.68

The circulating current loss in the formed winding is the largest, the value is 355.68W. Although the formed winding in PMSM has great advantages, its circulating current loss is still an important issue. So, it is necessary to analyze influencing factors of the circulating current loss in the formed winding.

IV. INFLUENCING FACTORS OF CIRCULATING CURRENT LOSS IN THE FORMED WINDING

The parallel strands in the formed winding are respectively at different positions in the slot. Besides, the slot leakage magnetic field is not uniformly distributed, resulting in different leakage magnetic fluxes in the strands. The leak-age inductance potential induced in the strands is different, so there is a potential difference between the strands. Parallel joints connect the ends of the strands, so there is a circulating current in the strands. The two main influencing factors of the circulating current loss are the slot leakage magnetic field and the position of the strands in the slot.

The distribution of the leakage magnetic field in the slot is different along with the slot height, and the circulating current loss in different slot height directions is different. PMSM with different winding arrangements have different number of parallel strands, slot widths, and rated currents, resulting

in different circulating current loss. The number of parallel strands is different, so the position of the magnetic field in the slot where the strand is located is also different. Different slot widths lead to different distribution of magnetic field leakage in the slot. The stator current is different, so the degree of magnetic field distortion is also different. In this section, the field-circuit coupling method is applied to analyze the influence of the number of parallel strands, the slot width, and the input current on the circulating current loss in the formed winding.

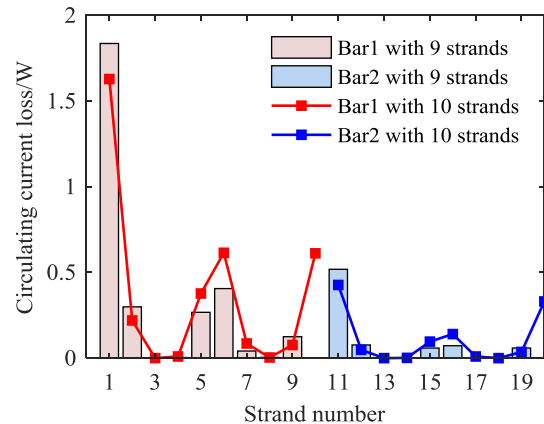


FIGURE 18. Circulating current loss of upper winding with 9 strands.

A. NUMBER OF PARALLEL STRANDS

Taking the integer slot PMSM as the research object, the number of parallel strands changes from 10 to 9. Ensure that the positions of the other 9 strands remain unchanged, and remove the No. 10 and No. 20 strands of each layer of winding. The stator current is the same as that of 10 strands in parallel. The circulating current loss distribution of the upper winding with different parallel strands is shown in Fig. 18. There is a strand at the same slot height, the circulating current loss distribution is not a “W”-shaped distribution. When the stator current and structure are unchanged, the leakage magnetic field in the slot is basically unchanged. When 9 strands in parallel, the position of each strand in the slot remains unchanged, and the circulating current loss of a single strand has a tiny change. Since the circulating current loss of the 10th and the 20th strand in each layer is disappear, the circulating current loss is reduced accordingly. The circulating current loss of 9 strands in parallel is less.

In the condition of constant electric density, change the number of parallel strands, from the original 10 strands to 8 and 6, respectively. Keep the stator structure and the input current unchanged, and the degree of distortion of the leakage magnetic field in the slot is the same. The number of parallel strands changes, and the position of each strand in the slot changes. Therefore, the strand current changes, and the circulating current loss changes accordingly.

The circulating current loss of the upper winding in the slot corresponding to the strands with different numbers of parallel strands are shown in Fig. 19. The distribution trend

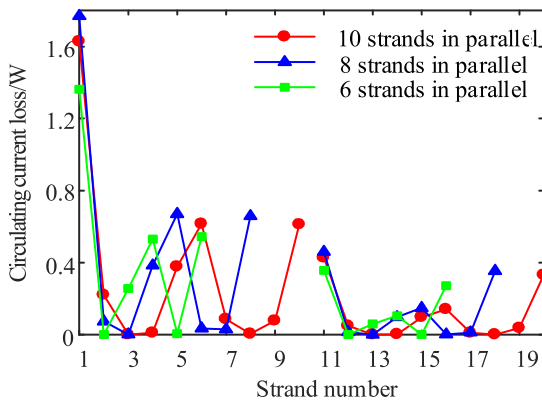


FIGURE 19. Circulating current loss of the upper winding.

of circulating current loss in the slot of stator bars with different numbers of parallel strands is the same, and they all show a “W”-shaped distribution. However, the position of each strand in the slot is different, and the closer to the slot, the greater the difference in circulating current loss.

TABLE 4. Circulating current loss of integer slot PMSM with different number of parallel strands.

	Single slot circulating current loss(W)	Total circulating current loss(W)
10 strands	4.94	355.68
8 strands	4.92	354.24
6 strands	3.65	262.80

The circulating current loss with different parallel strands are shown in Table 4. It can be seen from Table 4 that the number of parallel strands increases, and the circulating current loss increases. However, the circulating current loss increases nonlinearly with the increase of the number of parallel windings. And the number of parallel strands increases to a certain extent, and the increase in circulating current loss is not obvious. The fewer the number of parallel strands, the smaller the circulation loss. However, when selecting the number of parallel strands in the stator bar, the eddy current loss that cannot be ignored in the strands should also be considered.

B. SLOT WIDTH

The distribution of leakage magnetic field in the slot will vary with the width of the slot opening. PMSM with the formed winding adopt open slot stator structure, and the width of the slot directly determines the slot opening width. According to the analysis of equation (9), the stator slot width has a great influence on the leakage inductance potential. The slot width is inversely proportional to the leakage inductance potential of the slot. As the slot width increases, the slot leakage inductance potential decreases, the potential difference between the strands decrease. The strand current decreases, and the circulating current loss decreases accordingly. The distribution of the circulating current loss in the upper winding and the

lower winding for the formed winding PMSM with different slot width is shown in Table 5.

TABLE 5. Circulating current loss of PMSM with different slot width.

	bs0=6.2mm	bs0=6.5mm	bs0=7mm
Circulating current loss of upper winding (W)	4.72	4.28	3.77
Circulating current loss of lower winding (W)	0.22	0.19	0.15
Total circulating current loss (W)	4.94	4.47	3.92

It can be seen from Table 5 that, regardless of the upper winding or the lower winding, the circulating current loss tends to decrease with the increase of the slot width. As the slot width increases, the potential difference between the strands decreases. So the circulating current loss decreases accordingly. At the beginning of the design of the formed winding PMSM, it is of great significance to select the appropriate slot width to reduce the circulating current loss.

The formed winding PMSM adopts a rectangular open slot structure, and the slot width is the same as the slot opening width. The larger the slot width, the smaller the circulating current loss. However, if the slot opening is too wide, the magnetic density of the stator teeth will be too high, which will affect the performance of the formed winding PMSM. Besides, the size of the stator teeth will also affect the mechanical strength of the PMSM. Therefore, comprehensive consideration should be taken to select the slot width of the formed winding PMSM.

C. CURRENT IN THE STATOR BAR

During the actual operation of the PMSM, operating conditions will vary with the requirements of the load. When the interior PMSM generates different torques, the required current is different. The magnitude of the stator current is different, and the distortion of the leakage magnetic field in the slot is different, which affects the circulating current loss between the strands. Taking the integer slot formed winding PMSM as an example, the simulation analysis of the rated operating condition and heavy load condition are carried out. The distribution of the leakage magnetic field in the slot is shown in Fig. 20. From Fig. 20, it can be seen that the magnetic field distortion is serious under heavy load condition, and the content of the leakage magnetic field in the slot increases.

The circulating current loss distributions of the upper and lower winding in the slot under different working conditions are shown in Fig. 21. When the PMSM is working in heavy load condition, the leakage magnetic field in the slot has a more significant impact on the strands. In this case, regardless of the upper winding or the lower winding, the circulating current loss of each strand is obviously more remarkable than the rated working condition. And The circulating current loss in one slot of the formed winding PMSM in the heavy load

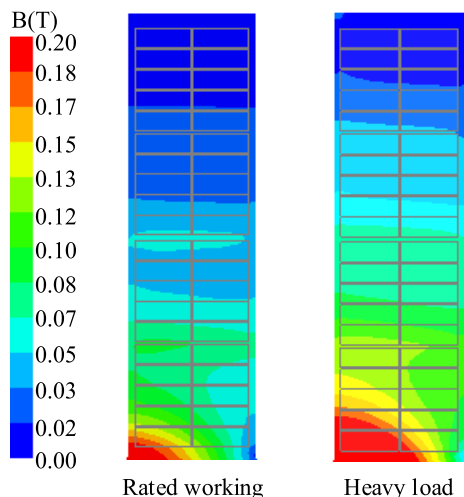


FIGURE 20. Magnetic field distribution in different working conditions.

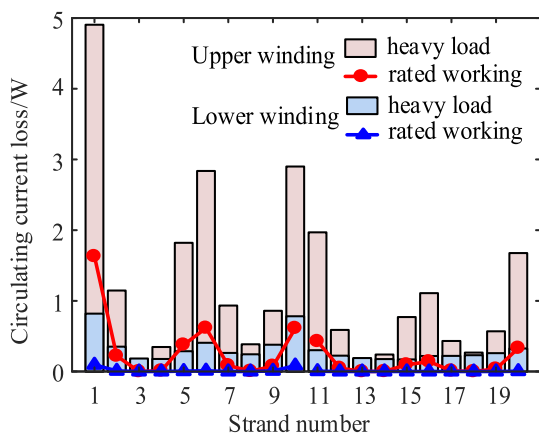


FIGURE 21. Circulating current loss in different working conditions.

condition is about 30.31W, which is much larger than that of the rated working condition.

V. CONCLUSION

This paper studied the circulating current loss in the formed winding of PMSM. Firstly, the no-load magnetic field of an integer slot and a fractional slot formed winding PMSM were analyzed. Then two commonly used methods for calculating circulating current loss were introduced and compared. The field-circuit coupling finite element method was applied to calculate the circulating current loss in the formed winding of PMSM. Finally, the influencing factors of circulating current loss were studied in detail. The main conclusions are as follows:

1) When the power, the main frame size, and the rotor magnetic circuit structure remain unchanged, the slot-pole combination affects the air gap magnetic density and the slot leakage magnetic field. The no-load air gap magnetic density fundamental wave amplitude of the integer slot PMSM is 0.78T, and the harmonic distortion rate is 19.75%, which are all smaller than the fractional slot PMSM.

2) Based on the principle that the power, rotor and main frame size are the same, the circulating current loss of PMSM with different slot-pole combination is different. Compared with the integer slot PMSM, the total circulating current loss of the fractional slot PMSM is smaller. The total circulating current loss of the fractional slot PMSM is 287.82W, which is only 80% of the integer slot PMSM.

3) The number of parallel strands, the slot width, and the stator current affect the circulating current loss. The circulating current loss of the PMSM with six strands in parallel is only 74% of 10 strands. The circulating current loss of the slot width with 7mm is only 79% of the slot width with 6.2mm. And the circulating current loss of PMSM under heavy load is about six times that under rated conditions. The fewer the parallel strands, the greater the slot width, the smaller the stator current, the smaller the circulating current loss in the formed winding will be.

REFERENCES

- [1] X. Sun, Z. Shi, G. Lei, Y. Guo, and J. Zhu, "Multi-objective design optimization of an IPMSM based on multilevel strategy," *IEEE Trans. Ind. Electron.*, vol. 68, no. 1, pp. 139–148, Jan. 2021, doi: 10.1109/TIE.2020.2965463.
- [2] K. Diao, X. Sun, G. Lei, G. Bramerdorfer, Y. Guo, and J. Zhu, "System-level robust design optimization of a switched reluctance motor drive system considering multiple driving cycles," *IEEE Trans. Energy Convers.*, vol. 36, no. 1, pp. 348–357, Mar. 2021, doi: 10.1109/TEC.2020.3009408.
- [3] S. S. Babu and A. Sukesh, "Current programmed controlled DC-DC converter for emulating the road load in six phase induction motor drive in electric vehicle," in *Proc. Int. Conf. Power Electron. Renew. Energy Appl. (PEREA)*, Kannur, India, Nov. 2020, pp. 1–6, doi: 10.1109/PEREA51218.2020.9339779.
- [4] K. Diao, X. Sun, G. Lei, Y. Guo, and J. Zhu, "Multiobjective system level optimization method for switched reluctance motor drive systems using finite-element model," *IEEE Trans. Ind. Electron.*, vol. 67, no. 12, pp. 10055–10064, Dec. 2020, doi: 10.1109/TIE.2019.2962483.
- [5] F. Zhang, D. Gerada, Z. Xu, C. Liu, H. Zhang, T. Zou, Y. C. Chong, and C. Gerada, "A thermal modelling approach and experimental validation for an oil spray-cooled hairpin winding machine," *IEEE Trans. Transport. Electric.*, early access, Mar. 19, 2021, doi: 10.1109/TTE.2021.3067601.
- [6] A. Arzillo, S. Nuzzo, P. Braglia, G. Franceschini, D. Barater, D. Gerada, and C. Gerada, "An analytical approach for the design of innovative hairpin winding layouts," in *Proc. Int. Conf. Electr. Mach. (ICEM)*, Aug. 2020, pp. 1534–1539, doi: 10.1109/ICEM49940.2020.9270927.
- [7] G. Berardi, S. Nategh, N. Bianchi, and Y. Thioliere, "A comparison between random and hairpin winding in e-mobility applications," in *Proc. IECON*, Singapore, 2020, pp. 815–820, doi: 10.1109/IECON43393.2020.9252629.
- [8] M. S. Islam, I. Husain, A. Ahmed, and A. Sathyan, "Asymmetric bar winding for high-speed traction electric machines," *IEEE Trans. Transport. Electric.*, vol. 6, no. 1, pp. 3–15, Mar. 2020, doi: 10.1109/TTE.2019.2962329.
- [9] H. Sano, T. Aasanuma, H. Katagiri, M. Miwa, K. Semba, and T. Yamada, "Loss calculation of bar-wound high-power-density PMSMs with massively parallel processing," in *Proc. IEEE Int. Electr. Mach. Drives Conf. (IEMDC)*, May 2017, pp. 1–6, doi: 10.1109/IEMDC.2017.8002252.
- [10] C. Du-Bar and O. Wallmark, "Eddy current losses in a hairpin winding for an automotive application," in *Proc. 13th Int. Conf. Electr. Mach. (ICEM)*, Sep. 2018, pp. 710–716, doi: 10.1109/ICELMACH.2018.8507265.
- [11] A. Lehtikoinen and A. Arkkio, "Efficient finite-element computation of circulating currents in thin parallel strands," *IEEE Trans. Magn.*, vol. 52, no. 3, pp. 1–4, Mar. 2016, doi: 10.1109/TMAG.2015.2481934.
- [12] H. Gao, Z. Zhang, C. Wang, Y. Liu, and W. Geng, "Loss analysis and efficiency optimization of ironless stator axial flux permanent magnet in-wheel machine," in *Proc. CSEE*, Oct. 2020, pp. 1–11, doi: 10.13334/j.0258-8013.pcsee.200768.

- [13] L. Yang, J. Zhao, X. D. Liu, A. Haddad, J. Liang, and H. Hu, "Effects of manufacturing imperfections on the circulating current in ironless brushless DC motors," *IEEE Trans. Ind. Electron.*, vol. 66, no. 1, pp. 338–348, Jan. 2019, doi: [10.1109/TIE.2018.2826474](https://doi.org/10.1109/TIE.2018.2826474).
- [14] Y. Yu, D. Liang, Z. Liang, and Q. Ze, "Calculation for stator loss of high-speed permanent magnet synchronous machine in torque-speed envelope and restraint approach for circulating current in windings," *CES TEMS*, vol. 2, no. 2, pp. 211–219, Jun. 2018, doi: [10.30941/CES-TEMS.2018.00026](https://doi.org/10.30941/CES-TEMS.2018.00026).
- [15] J. J. Pérez-Loya, C. J. D. Abrahamsson, and U. Lundin, "Electromagnetic losses in synchronous machines during active compensation of unbalanced magnetic pull," *IEEE Trans. Ind. Electron.*, vol. 66, no. 1, pp. 124–131, Jan. 2019, doi: [10.1109/TIE.2018.2827991](https://doi.org/10.1109/TIE.2018.2827991).
- [16] K. Yamazaki, T. Furuhashi, H. Yui, H. Ohguchi, S. Imamori, and M. Shuto, "Analysis and reduction of circulating current loss of armature wires in permanent magnet synchronous machines," *IEEE Trans. Ind. Appl.*, vol. 55, no. 6, pp. 5888–5896, Nov. 2019, doi: [10.1109/TIA.2019.2940425](https://doi.org/10.1109/TIA.2019.2940425).
- [17] T. Noguchi and T. Komori, "Eddy-current loss analysis of copper-bar windings of ultra high-speed PM motor," in *Proc. Int. Conf. Electr. Syst. Aircr., Railway, Ship Propuls. Road Vehicles (ESARS)*, Aachen, Germany, Mar. 2015, pp. 1–6, doi: [10.1109/ESARS.2015.7101455](https://doi.org/10.1109/ESARS.2015.7101455).
- [18] M. Vetuschi and F. Cupertino, "Minimization of proximity losses in electrical machines with tooth-wound coils," *IEEE Trans. Ind. Appl.*, vol. 51, no. 4, pp. 3068–3076, Jul./Aug. 2015, doi: [10.1109/TIA.2015.2412095](https://doi.org/10.1109/TIA.2015.2412095).
- [19] D. Wang, Y. Liang, L. Gao, X. Bian, and C. Wang, "A new global transposition method of stator winding and its loss calculation in AC machines," *IEEE Trans. Energy Convers.*, vol. 35, no. 1, pp. 149–156, Mar. 2020, doi: [10.1109/TEC.2019.2947082](https://doi.org/10.1109/TEC.2019.2947082).
- [20] C. Roth, F. Birnkammer, and D. Gerling, "Analytical model for AC loss calculation applied to parallel conductors in electrical machines," in *Proc. ICEM*, 2018, pp. 1088–1094, doi: [10.1109/ICELMACH.2018.8507237](https://doi.org/10.1109/ICELMACH.2018.8507237).
- [21] F. Birnkammer, J. Chen, D. B. Pinhal, and D. Gerling, "Influence of the modeling depth and voltage level on the AC losses in parallel conductors of a permanent magnet synchronous machine," *IEEE Trans. Appl. Supercond.*, vol. 28, no. 3, pp. 1–5, Apr. 2018, doi: [10.1109/TASC.2018.2801292](https://doi.org/10.1109/TASC.2018.2801292).
- [22] A. Bardalai, D. Gerada, D. Golovanov, Z. Xu, X. Zhang, J. Li, H. Zhang, and C. Gerada, "Reduction of winding AC losses by accurate conductor placement in high frequency electrical machines," *IEEE Trans. Ind. Appl.*, vol. 56, no. 1, pp. 183–193, Jan. 2020, doi: [10.1109/TIA.2019.2947552](https://doi.org/10.1109/TIA.2019.2947552).
- [23] Y. Liang, X. Qiao, X. Bian, and J. Li, "Improved method of leakage susceptible electromotive potential to calculate strand current and circulation current losses in transposition windings," *Trans. CES*, vol. 32, no. 17, pp. 164–171, 2017, doi: [10.19595/j.cnki.1000-6753.tecs.161053](https://doi.org/10.19595/j.cnki.1000-6753.tecs.161053).
- [24] M. Popescu and D. G. Dorrell, "Proximity losses in the windings of high speed brushless permanent magnet AC motors with single tooth windings and parallel paths," *IEEE Trans. Magn.*, vol. 49, no. 7, pp. 3913–3916, Jul. 2013, doi: [10.1109/TMAG.2013.2247382](https://doi.org/10.1109/TMAG.2013.2247382).
- [25] S. Skoog and A. Acquaviva, "Pole-slot selection considerations for double layer three-phase tooth-coil wound electrical machines," in *Proc. 13th Int. Conf. Electr. Mach. (ICEM)*, Alexandroupoli, Greece, Sep. 2018, pp. 934–940, doi: [10.1109/ICELMACH.2018.8506772](https://doi.org/10.1109/ICELMACH.2018.8506772).
- [26] X. Fan, B. Zhang, R. Qu, D. Li, J. Li, and Y. Huo, "Comparative thermal analysis of IPMSMs with integral-slot distributed-winding (ISDW) and fractional-slot concentrated-winding (FSCW) for electric vehicle application," *IEEE Trans. Ind. Appl.*, vol. 55, no. 4, pp. 3577–3588, Jul./Aug. 2019, doi: [10.1109/TIA.2019.2903187](https://doi.org/10.1109/TIA.2019.2903187).
- [27] K. Wang and H. Lin, "A novel 24-slot/10-pole dual three-phase fractional-slot overlapped winding for low non-working space harmonics and stator modularization," *IEEE Access*, vol. 8, pp. 85490–85503, 2020, doi: [10.1109/ACCESS.2020.2992258](https://doi.org/10.1109/ACCESS.2020.2992258).
- [28] E. Fornasiero, L. Alberti, N. Bianchi, and S. Bolognani, "Considerations on selecting fractional-slot nonoverlapped coil windings," *IEEE Trans. Ind. Appl.*, vol. 49, no. 3, pp. 1316–1324, May-Jun. 2013, doi: [10.1109/TIA.2013.2251853](https://doi.org/10.1109/TIA.2013.2251853).
- [29] W. Gul, Q. Gao, and W. Lenwari, "Optimal design of a 5MW double stator single rotor permanent magnet synchronous generator for offshore direct drive wind turbines using the genetic algorithm," in *Proc. 21st Int. Conf. Electr. Mach. Syst. (ICEMS)*, Jeju, South Korea, Oct. 2018, pp. 149–155, doi: [10.23919/ICEMS.2018.8549413](https://doi.org/10.23919/ICEMS.2018.8549413).



JIA LIU was born in Daqing, China, in 1996. She is currently pursuing the M.S. degree in electrical machines with Harbin University of Science and Technology, Harbin, China. Her research interests include electromagnetic analysis and loss calculation on electrical machines and design on permanent magnet synchronous motors.



YANPING LIANG was born in Harbin, China, in 1963. She received the M.S. and Ph.D. degrees in electrical machines from Harbin University of Science and Technology, Harbin, in 1988 and 2005, respectively.

She is currently a Professor with Harbin University of Science and Technology. Her research interests include electrical machine electromagnetic theory and design, large generator electromechanical energy conversion, and electromagnetic field calculation.



PEIPEI YANG was born in Hebei, China, in 1993. She is currently pursuing the Ph.D. degree in electrical machines with Harbin University of Science and Technology, Harbin, China. Her research interests include electromagnetic and thermal analysis on electrical machines.



WEIHAO WANG was born in Heihe, China, in 1998. He received the B.S. degree from Harbin University of Science and Technology, Harbin, China, in 2019, where he is currently pursuing the M.S. degree in electrical engineering. His research interests include the electromagnetic calculation and windings fault diagnosis.



FUCHAO ZHAO was born in Qiqihaer, China, in 1996. He is currently pursuing the M.S. degree in electrical machines with Harbin University of Science and Technology, Harbin, China. His research interests include electromagnetic and field and thermal analysis on electrical machines.



KANGWEN XU was born in Heilongjiang, China, in 1997. He received the B.S. degree from Harbin University of Science and Technology, Harbin, China, in 2019, where he is currently pursuing the M.S. degree in electrical engineering. His research interests include the winding design, simulating calculation, and optimization method.